

# Visual Analytics of Multivariate Networks with Representation Learning and Composite Variable Construction

Hsiao-Ying Lu, Takanori Fujiwara, Ming-Yi Chang, Yang-chih Fu, Anders Ynnerman, and Kwan-Liu Ma

**Abstract**—Multivariate networks are commonly found in real-world data-driven applications. Uncovering and understanding the relations of interest in multivariate networks is not a trivial task. This paper presents a visual analytics workflow for studying multivariate networks to extract associations between different structural and semantic characteristics of the networks (e.g., what are the combinations of attributes largely relating to the density of a social network?). The workflow consists of a neural-network-based learning phase to classify the data based on the chosen input and output attributes, a dimensionality reduction and optimization phase to produce a simplified set of results for examination, and finally an interpreting phase conducted by the user through an interactive visualization interface. A key part of our design is a composite variable construction step that remodels nonlinear features obtained by neural networks into linear features that are intuitive to interpret. We demonstrate the capabilities of this workflow with multiple case studies on networks derived from social media usage and also evaluate the workflow through an expert interview.

**Index Terms**—Interpretability, network representation learning, composite variable, density scatterplots, neural networks, visualization.

## 1 INTRODUCTION

Multivariate networks [30] consisting of both topological and semantic information can model complex relations between real-world entities. One common analysis task performed on multivariate networks is to understand associations among structural and semantic characteristics of networks [2, 11, 30]. For example, from social media usage data, analysts would want to see how likely each possible combination of individual characteristics (e.g., age, gender, and extraversion) and their friendship structures is related to their addiction level to social media. Such analysis can be very complicated when the associations underlie intertwining social facts.

To aid in analysis of multivariate networks, researchers have introduced visual analytic support, including network layouts considering semantic information, interactive simplification, and incorporation of coordinated views [30, 46]. Among others, utilizing network representation learning (NRL) [64] is one promising approach as it can capture latent features of multivariate networks and highlight essential aspects that should be examined with visualizations. Existing visual analytics methods [18, 19, 40, 41, 55, 58] utilize NRL methods that learn networks' general representations—consisting of a set of features that summarizes overall network information without a certain analysis focus. However, when analysts have a specific interest (e.g., the friendship structure's influences on the addiction level to social media), a general-purpose NRL would not be effective as it is not particularly designed for such a case, and thus may fail to capture features important for the corresponding interest.

On the other hand, as seen in the machine learning field, NRL using neural networks (NNs) can learn representations specific for an analysis focus by using appropriate loss functions [24]. While these representations are suitable for fully automated analyses, such as network classification, it is often difficult for analysts to interpret the extracted features. This is not preferable for the case where the analysts want to be involved in and derive insights during the analysis process.

To address the aforementioned two-folded problems, we introduce a visual analytics workflow that provides network representations specific to a task of uncovering the structural and semantic associations

from multivariate networks as well as an interpretation support for the analysis results. For NRL, we train an NN-based model that is designed to classify values of a user-selected attribute (e.g., whether the addiction level to social media is high or low). Through the training, the model generates latent features that are highly related to the selected attribute.

For the interpretation of the obtained network representations, we employ dimensionality reduction (DR), interactive visualization, and composite variables [56]. To help analysts assess the quality of the representations, we simplify the latent features with a linear DR method (specifically, linear discriminant analysis or LDA). We then visualize the information of the simplified features in a 2D plot, where the distribution of networks or their elements (i.e., nodes and links) is shown along the direction related to the classification. From this plot, analysts can judge which part of networks or elements (e.g., subjects with age 20–30) likely holds more clear associations with the selected attribute, which is almost infeasible when only relying on the classification quality measures. In addition, we introduce a mechanism of composite variable construction to explain the meanings of the network representations. The mechanism first suggests network structures and attributes highly related to the representations by utilizing a model-agnostic interpretation method, the SHAP [39]. Then, after allowing analysts to interactively select the structures and attributes from the suggestion, an optimization method automatically generates a composite variable that resembles the representation extracted by the NNs. By examining this composite variable, analysts can understand the relationships among the selected attributes and the other related information.

To effectively analyze the associations between the composite variable and network representation, we develop a new density scatterplot, named *two-class density scatterplot*, that can clearly depict a trend of the data distribution as well as inform the mixture and separation of two classes. Incorporating the two-class density scatterplot, we develop an interactive interface linking all the visualizations to support the above visual analytics workflow, and demonstrate the capabilities of the workflow with three case studies using two real-world datasets on social media usage. Moreover, we conduct an expert interview to validate the usability of the workflow.

In summary, we consider our primary contributions to be:

- a visual analytics workflow considering both generation and interpretation of network representations that are expressive for user-specified analysis targets;
- a mechanism of composite variable construction, where we support attribute selection and attribute weight optimization to assist the interpretation with a combinational influence from multiple attributes; and
- a two-class density scatterplot as a versatile visualization to re-

- Hsiao-Ying Lu and Kwan-Liu Ma are with University of California, Davis. E-mail: {hyllu, klma}@ucdavis.edu.
- Takanori Fujiwara and Anders Ynnerman are with Linköping University. E-mail: {takanori.fujiwara, anders.ynnerman}@liu.se.
- Ming-Yi Chang is with Fu Jen Catholic University. E-mail: mychang@mail.fju.edu.tw.
- Yang-chih Fu is with Academia Sinica. E-mail: fuyc@gate.sinica.edu.tw.

view individual- and group-level data patterns with binary class information.

## 2 RELATED WORK

Our work is closely related to two research topics studied in the visualization field: NRL and the interpretation of learned representations. For the broader discussion on visualizations for analyzing networks and interpreting machine learning results, refer to existing surveys [4, 9, 30, 42].

### 2.1 Learning Network Representations

NRL aims to generate a set of low-dimensional vectors (also called representation) that captures certain important characteristics of networks, nodes, or links [64]. The representation is usually learned for downstream tasks, such as node classification and link prediction. Various NRL methods are developed, including node2vec [22], graph convolutional networks [31], graph neural networks (GNNs) with the self-attention [63], to name but a few [64].

The researchers have been utilizing NRL together with visualization to interactively examine large-scale, complex network datasets. For example, Freire et al. [14] represented one network by a set of network statistics (e.g., degree distribution) and organized many networks in a tabular interface to compare them. Gove [21] suggested several network-level features (e.g., density) that are easier to interpret and faster to compute for interactive visualization. To capture the network connectivity at a detailed level, the researchers measured the occurrences of graphlets [51] (small, connected, non-isomorphic subgraph patterns in a network). The graphlet-based representations have been used to identify visually similar networks [26, 34, 60]. When node correspondence exists among networks, another common approach is directly applying DR methods to networks' adjacency matrices to obtain a representation that shows the similarities of networks [3, 15]. Van den Elzen et al. [58] took a similar DR approach but they further incorporated network statistics, such as the number of nodes. Martins et al. [40, 41] used DR to lay out network nodes based on their structural and semantic similarities.

Similar to ours, recently, a few works employed NN-based NRL. Fujiwara et al. [19] introduced contrastive NRL (cNRL) by integrating a variant of GNNs and contrastive learning [66]. cNRL extracts a representation of two networks, where salient characteristics in one network relative to another are highlighted. Utilizing linear DR, they further designed an interpretable cNRL method and enhanced it with interactive visualizations [18]. Song et al. [55] used GNNs to support interactive subgraph pattern search, where GNNs are used to covert each network in a comparable, fixed-length latent vector.

As stated, unlike the above approaches, we use NN-based NRL to obtain representations that are specifically for uncovering the relations of interest in multivariate networks. Also, we address the interpretation of the representations with the composite variable construction, which is easier to examine when compared with the approaches referring to coefficients in the linear DR results [18, 19].

### 2.2 Interpreting Representations

Although the interpretation of network representations is still sparsely studied (e.g., [18]), various interpretation methods are developed for high-dimensional data's representations which are often extracted by using DR methods or NNs. Generally, existing methods can be categorized into two approaches: (1) identifying essential information to specific patterns found in complex representations (i.e., post-hoc explanation approach) and (2) constructing simple, interpretable representations during a learning phase (i.e., explainability-by-design approach [25]).

Many visual analytics methods for the interpretation of nonlinear DR results are corresponding to the first approach. For example, researchers visually identified attributes that are highly influential on the cluster formation in DR results from related statistical charts (e.g., boxplots of the attribute distributions for each cluster) [33, 44]. As these univariate statistical charts could be insufficient to capture the characteristics of

clusters, some researchers further considered the combinational influences from multiple attributes [16, 29, 57, 65]. For example, to identify such influences, Joia et al. [29] applied PCA to each cluster, instead of the entire data. While the above works are mainly to understand clusters, several methods focused more on understanding other local patterns [7, 10, 13].

There are a relatively small number of visual analytics works taking the explainability-by-design approach. Knittle et al. [32] used NNs consisting of one hidden layer with a small number of NN nodes to extract nonlinear representations that relate input attributes to a target output attribute. These simple NNs allowed them to review all representations held by the NN nodes and identified those showing clear relationships between the input and target attributes. Then, they constructed a stacked histogram for each input attribute to visually convey such relationships in detail. Gleicher [20] produced simple composite variables that are to classify a user-selected attribute. To craft such composite variables, Gleicher performed an exhaustive search for the selection of variables and applied support-vector machines to adjust the weight for each variable while considering a balance between, for example, simplicity and expressiveness.

In terms of using NNs to extract the input-output relationships, the work by Knittle et al. [32] is closely related to ours. However, their interpretation of the obtained representations is based only on univariate value distributions, which is insufficient when NNs capture complex input-output relationships. Similar to Gleicher's work [20], our work crafts simple composite variables, but we do not involve the computationally expensive exhaustive search. Instead, we rank variables based on their contributions to the NNs' predictions and involve analysts' knowledge to select attributes of interest.

## 3 METHODOLOGY

This section introduces our visual analytics workflow.<sup>1</sup> We first describe design considerations of the workflow, which are identified based on our literature survey in Sect. 2 and targeted analysis on multivariate networks (for the detailed definition of multivariate networks, refer to the introduction by Kerren et al. [30]). We then provide an overview of the workflow, followed by the details of each step.

### 3.1 Design Considerations

The following five design considerations (DCs) are identified to support the analysis task for understanding the relations of interest and to fill the analytical gap that is not covered by existing methods.

**DC1: Flexibility.** Reviewing multivariate networks requires analyses from multiple aspects, such as the relationships among structural information as well as semantic information (e.g., network node's age and gender). Also, based on the analysis purpose and available datasets, analysts often want to investigate networks from different levels, such as node, link, and network levels. The workflow should provide the flexibility to conduct analyses from multiple aspects at various levels.

**DC2: Expressivity.** Our work's main objective is to effectively support the stated analysis—examining the relationships among the target (e.g., the addiction level to social media) and other related information (e.g., gender, age, and the number of friends). The workflow should be able to extract features that are expressive for this analysis task (i.e., containing important information for the task) rather than providing a general summary of the network information.

**DC3: Interpretability.** To gain insights through the analyses, the interpretation of results is essential. Because expressive features such as those extracted by NNs are often difficult to explain only with each individual attribute's influence, the workflow should provide more advanced interpretation support that considers the combined influence from multiple attributes.

**DC4: Tunability.** Conflict often exists between the expressiveness and interpretability of features (i.e., more expressive features are often more difficult to interpret). Also, the requirement for the interpretation's preciseness can differ by the analysis (i.e., more complicated but precise

<sup>1</sup>The related source code is available at <https://github.com/hylu1994/Network-CV>

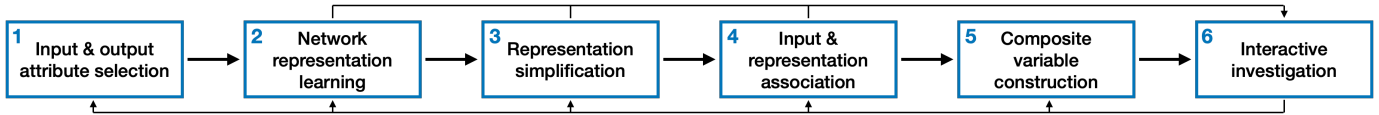


Fig. 1. The visual analytics workflow for understanding the relations in multivariate networks.

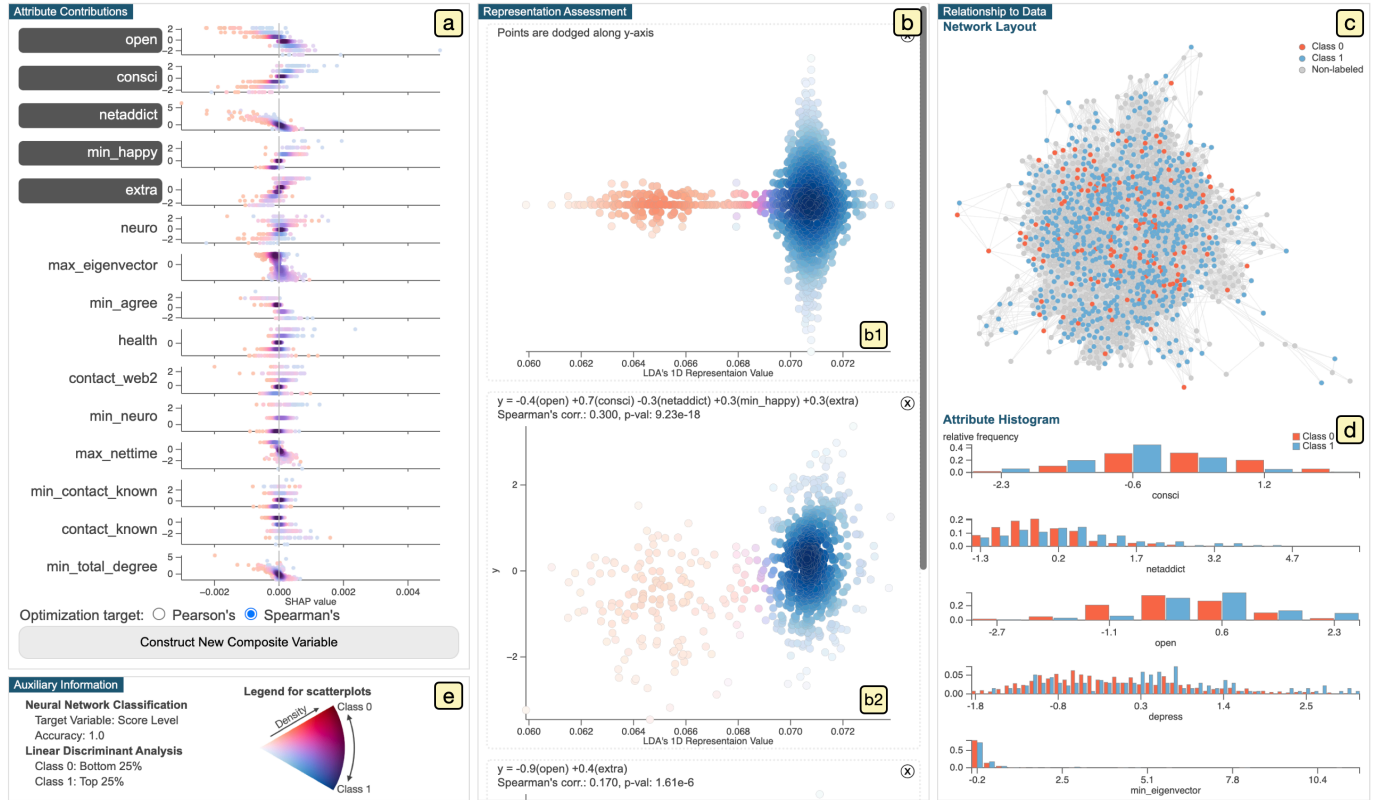


Fig. 2. The visual interface for facilitating interactive analysis using the workflow in Fig. 1. (a) Relating to Step 4, this view visualizes the input attributes' contributions to the 1D network representation. (b) The composite variables generated in Step 5 are shown as a list of scatterplots, where the 1D network representation and the composite variable correspond to  $x$ - and  $y$ -axes, respectively (see b2). As shown in b1, when a composite variable is not generated yet, a swarm-plot-like visualization presents the 1D network representation generated through Step 3 to help assess its quality. For a and b, we employ our two-class density scatterplots to depict density and class distribution information simultaneously. As shown in the fan-shape colormap in e, color lightness and hue are used to encode the density and the ratio of each class's density at each position, respectively. For example, in b2, we can see a high-density area mainly consisting of Class 1 (blue) at the right side as well as a clear separation between two classes (e.g., Class 0 (red) is mostly located at the left side). (c) A node-link diagram and (d) a set of histograms inform the network structure and attribute distributions, respectively. (e) Other auxiliary information is displayed, including the prediction accuracy of NNs trained for Step 2.

interpretation vs less precise but simple interpretation). The workflow should allow the analysts to control the balance of the expressiveness and interpretability and interactively examine the results based on their interests.

**DC5: Extensibility.** While we provide a concretized method for each step of the workflow, a different set of methods may be more suitable according to the characteristics of future datasets and analysis goals. The workflow should be extensible to incorporate new or different methods.

### 3.2 Workflow Overview

Fig. 1 shows our workflow for reviewing the relations embedded in multivariate networks. It consists of six steps that are performed first with a script for machine learning (Steps 1–4) and then with our user interface (UI) designed for visual analysis (Steps 5–6), as shown in Fig. 2.<sup>2</sup> As we describe in Sect. 3.4.1, we extract structural information as a set of network measures (e.g., degree and betweenness centralities)

for each element (i.e., node, link, or network); thus, in the following, we use a term, attribute, to indicate both extracted structural (e.g., degree) and semantic information (e.g., age).

**Step 1.** The workflow begins with the selection of input attributes and one output/target attribute. For example, to know how students' grades in a school class are related to their surrounding conditions, an analyst may choose their attending class size, mental health status (e.g., depression level), and centrality in the social media connections (e.g., degree) as inputs and their grade as an output.

**Step 2.** NRL is performed based on the selected inputs and output. A network representation is generated by an NN trained to predict the output from the input values. The representation, thus, can be specific to relations of the analyst's interest.

**Step 3.** This step compresses the dimensionality of the network representation from many dimensions into one while preserving the prediction quality as much as possible. This makes the remaining steps simpler to complete and the related results easier to interpret.

**Step 4.** This step evaluates and ranks each input attribute's contribution to the construction of the 1D compressed representation. The obtained ranks can be considered as the recommendation levels of the

<sup>2</sup>The demonstration of the UI can be found at <https://github.com/hylu1994/Network-CV>

inclusion of the corresponding attributes for the composite variable construction in Step 5.

**Step 5.** Finally, based on the recommendation levels and interests, the analyst manually selects a small set of attributes (e.g., 2–5 attributes) and runs a composite variable construction algorithm. The optimized composite variable (e.g., the y-axis in Fig. 2-b2) maximally resembles the 1D compressed representation (e.g., the x-axis in Fig. 2-b2). This composite variable provides an intuitive explanation of how the selected small set of attributes is related to the output/target attribute.

**Step 6.** The UI in Fig. 2 visualizes the information related to each of the previous steps as well as the detailed structural and semantic information of the multivariate network. By interactively reviewing these pieces of information, the analyst can gain analytical insights or adjust the settings used for the previous steps based on their analysis interests (the backward arrows in Fig. 1). The analyst can also refer to the UI at each step (the forward arrows in Fig. 1).

### 3.3 Datasets

In the rest of this section, our explanations refer to a real-world dataset, Dataset I, described below as a concrete analysis target. We also analyze Datasets I and II in our case studies (Sect. 4).

**Datasets: College students and adults’ network resources.** We analyze multivariate networks derived from the Facebook usage and survey data of two representative cohorts, senior college students and sampled adults in Taiwan. For **Dataset I (senior college students)** [8], the survey is on topics related to their school life, such as their personalities, moods, and grades. **Dataset II (Taiwanese adults)** [35] uses Taiwan Social Change Survey, which includes important network-related topics, such as core discussion networks and network resources, as well as personal attributes, such as their backgrounds, personalities, mood, and social lives. With Facebook usage data, we represent each respondent as a network node and create a link based on the interactions on Facebook. We construct an undirected link if a “like”, “comment”, or “tagged” was made between respondents on a post. We can consider such links as “friendships” in social media and 1-hop neighbors of each node as “friends”. We further use the answers for the survey as each node’s attributes.

Below, from Dataset I, we identify and review college students’ attributes that are highly related to their `scorelevel`, the past three years’ mean score levels reported on a scale of four from the top to bottom. While the resultant network consists of 1886 nodes, 64156 links, and over 200 survey-based attributes for each node, we picked 14 survey attributes related to this analysis.

### 3.4 Learning Representations

We explain Steps 1–3, where we learn representations from multivariate networks. To provide a concise explanation, here we describe each process for the case producing a latent vector for each node (i.e., node feature learning). However, our learning processes are generic enough to be adjusted to learn a latent vector for each link or network (DC1: Flexibility).

#### 3.4.1 Network Representation Learning

To allow analysts to select attributes related to the structural information in Step 1, similar to existing works [18, 58], we first precompute a set of network measures. For node feature learning, such measures can be degree, eigenvector, betweenness centralities, and many others [45].

Each of these centralities informs the importance of each node in a network from different aspects. Degree centralities, or node degrees (i.e., the number of links connected to each node), measure local importance of nodes in the network. Eigenvector centralities (i.e., the eigenvector corresponding to the greatest eigenvalue of the network’s adjacency matrix) are more suitable to show global importance of nodes as eigenvector centralities consider the transitive importance of links (e.g., a link connecting to a node with 100 links is more important than one with 1 link). Betweenness centralities (the number of shortest paths that pass through each node) show the importance of each node as a “bridge” connecting other nodes. For more details, refer to the introduction to network theory by Newman [45].

Furthermore, to capture more detailed-level structural information, we precompute advanced measures related to the statistics of each node’s neighbors, such as the mean, variance, and maximum of  $k$ -hop neighbors’ degrees. Such neighbor statistics can be also computed for semantic attributes (e.g., the mean age of neighbors). The neighbor statistics have been shown to be useful for various analytical tasks [18, 53]. For the precomputation, we specifically use DeepGL [53] to achieve fast computation while avoiding producing many redundant measures.

DeepGL summarizes 1-hop neighbors’ centrality/attribute values (called *base features*), using *relational functions*. For relational functions, we can specify multiple neighbor types (e.g., in-, out-, and total-neighbors) and aggregation functions (e.g., sum, mean, variance, and maximum). After obtaining the neighbor statistics for all nodes, DeepGL prunes redundant statistics that show similar value distributions to others. The strength of pruning can be controlled with a hyperparameter of DeepGL. Moreover, DeepGL can repeatedly apply the relational functions and pruning process to summarize farther neighbors’ features. For more details, refer to the work by Rossi et al. [53]. For Dataset I, as base features, we select 3 fundamental network centralities, degree, eigenvector, and betweenness, and the 14 survey attributes; then, we generate 1-hop total-neighbor statistics of the 17 attributes, resulting in 85 attributes in total after the pruning process.

After selecting input and output attributes in Step 1, we first apply the Z-score normalization to the attributes. We then train an NN to predict the output from input values, and extract representations from an NN layer (DC2: Expressivity). While we could predict an output value directly by designing the NN for a regression task, we categorize output values and perform binary classification of two value ends (e.g., top and bottom 25% of attribute values). Note that the classification is performed only on these ends, and thus unrelated instances are not involved in training. If we perform regression, instead of this process, the NN tries to fit all instances, resulting in a representation that might be mainly useful to predict values in the middle range (e.g., when fitting to the two ends is harder than the middle range). While we assume this focus on two ends is reasonable for many analyses, this setting can be easily changed based on the analysis interests. This design employing binary classification also allows a comparison of two categorical groups (e.g., students who major in engineering vs. business).

By default, we use a multi-layer perceptron (MLP) consisting of five fully-connected layers (one input, three hidden, and one output layers) and take the last hidden layer’s activations as the learned representation. We employ the leaky rectified linear unit as an activation function to obtain expressive representations by utilizing its nonlinearity. On the other hand, with the consideration of the balance between expressivity and interpretability, we keep the numbers of hidden layers and nodes small relative to the size of the input data. However, we should note that, for this step, it is acceptable to cause overfitting to some extent. As described in Sect. 3.4.2, we simplify this step’s high-dimensional network representation with linear transformation, which can mitigate overfitting when it occurs. With consideration for the next step, this NN-based learning step should rather focus on achieving an accurate alignment of the defined classes in the learned representation. When we have such an alignment, the NN’s classification accuracy should be high, which can be also checked in the UI, as shown in Fig. 2-e.

While the five-layer MLP is our default NN architecture, the analyst can easily replace it with more complex architecture (DC5: Extensibility). For example, when the analyst needs to capture nonlinear neighbor relations in a network, they can incorporate a GNN into the NN architecture. Also, as stated, the above process can be adjusted to learn latent vectors of links or networks. This can be achieved by replacing the precomputation of network measures, accordingly. For example, instead of the centralities, for network feature learning, we can extract the mean degree, the number of nodes, network diameter, etc. Then, we can apply the same procedure employing an NN.

### 3.4.2 Representation Simplification

We simplify the high-dimensional network representation into a 1D representation for the ensuing interpretation steps (DC3: Interpretability). Because the NN is trained for binary classification, this simplification is similar to the process NNs usually perform for the output layer: transforming the last hidden layer’s activations of multiple nodes into a single node at the output layer. Thus, we expect that even though the simplified representation is 1D, it can preserve sufficient information for the prediction (DC2: Expressivity).

A major difference from conventional NNs is that we employ linear transformation, instead of nonlinear transformation. For conventional NNs, a nonlinear activation function such as a sigmoid or softmax function is usually employed to encourage producing a value of 0 or 1 for classification. Consequently, the corresponding 1D representations would consist of many values close to 0 or 1. This close-to-discrete distribution makes it difficult not only to perform the optimization for the composite variable construction but also to observe patterns from visualizations shown in Fig. 2-b.

One way to obtain a 1D representation with linear transformation is using a linear activation function between the last hidden and output layers, as in NNs for regression tasks. However, as stated, we want to avoid directly performing regression in the NN. Instead, as a post-hoc process, we apply a DR method, specifically LDA, to the high-dimensional network representation. With the class information, LDA produces a low-dimensional representation that places instances in different classes as far as possible. To do so, LDA minimizes data variance within each class while maximizing the separation of each class’s centroid. The benefit of this post-hoc approach is that LDA can efficiently generate a 1D representation that is the global optimum solution for class separation.

However, similar to NNs, LDA can easily cause overfitting when the number of instances is small relative to the number of input features [23]. To solve this issue, we use an enhanced LDA, called regularized LDA, that has a regularization mechanism to avoid overfitting [23]. The use of regularized LDA brings an additional benefit for the post-hoc approach: the regularization strength can be controlled outside of the NN training process. While the L1 and L2 regularizations can be used for NNs to avoid overfitting, the hyperparameter adjustment for these often requires many trials and errors, and becomes time-consuming by retraining NNs many times. Applying regularization inside of LDA does not require retraining of NNs and LDA is computationally efficient; thus, we can adjust the regularization strength more conveniently (DC4: Tunability).

The quality of the 1D representation can be investigated with a swarm-plot-like visualization, as shown in Fig. 2-b1. This visualization shows an instance as a dot and a 1D representation value as an  $x$ -coordinate. Similar to the swarm plot [61],  $y$ -direction is used to pile up dots while involving positional jitters to mitigate overplotting within a limited vertical space. The resultant area height roughly shows the frequency/density around the corresponding  $x$ -coordinate as similar to a histogram. We select this instance/point-based visualization to keep it consistent with other visualizations using  $x$ -coordinates to represent the 1D representation values (e.g., Fig. 2-b2). As shown in the fan-shape colormap located at Fig. 2-e, the color of each dot shows the density and the ratio of each class’s density at the corresponding position, which we explain in Sect. 3.5.3. When the 1D representation has good quality, as seen in Fig. 2-b1, two classes (Class 0: red, Class 1: blue) should have small or no overlaps (note: overlapped parts have purple colors). When the quality is not satisfactory, the analyst can update the NN architecture and/or the selection of input and output attributes.

Before we chose the above architecture first applying an MLP and then LDA, we experimented with two alternative designs. As the first alternative design, we directly applied LDA to obtain the 1D representation. The result after directly applying LDA to the same dataset as Fig. 2-b is shown in Fig. 3-a. As this design does not utilize the strengths of NNs, the two classes are more mixed together when compared with Fig. 2-b. Second, we only used an MLP, in which a softmax activation function is used to output the 1D representation (unlike our approach using LDA for this step). The result shown

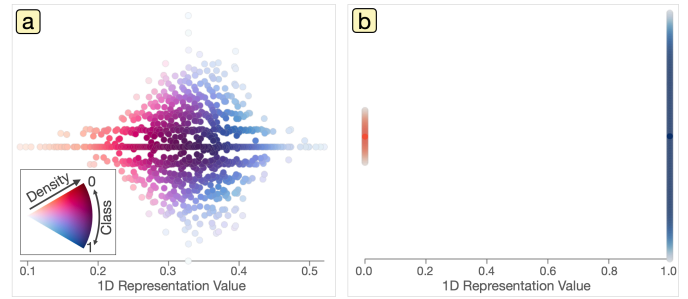


Fig. 3. The swarm-plot-like visualizations of the 1D representations generated by the designs using (a) only LDA and (b) only an MLP.

in Fig. 3-b exhibits the aforementioned issue of the close-to-discrete distributions, although the two classes are well separated. These two results show that our final design is better for providing a good balance of expressivity and interpretability.

## 3.5 Understanding Representations

We describe Steps 4 and 5, which are mainly for understanding the representation obtained through Steps 1–3.

### 3.5.1 Attribute Contribution Measurement

In Step 4, we extract each input attribute’s contribution to the 1D representation which can be considered as a latent space that disentangles the output attribute by referring to the input attributes. We utilize the attribute contribution to understand each attribute’s relationship to the output attribute—the interpretation from a single attribute level—as well as to recommend attributes for the composite variable construction—the interpretation considering the combinational attribute influences (DC3: Interpretability).

To measure the attribute contributions, we use the SHAP method [39]. By employing cooperative game theory, for each instance, the SHAP method calculates a measure, called the SHAP value, that shows an attribute’s contribution to a given target value (refer to [39] for details). In our case, we apply the SHAP method to a transferred model that combines the MLP trained in Step 2 and LDA trained in Step 3. Then, the SHAP value indicates how much having a corresponding attribute value contributes to moving an instance toward a positive direction of the 1D representation. For example, when instance A is age 25 and its SHAP value for the age attribute is 0.01, by having this age, instance A is placed at a more positive side of the 1D representation by the degree of 0.01.

As shown in Fig. 2-a, we visualize SHAP values with a set of scatterplots. Each row corresponding to one attribute shows a scatterplot where the  $x$ - and  $y$ -axes show the SHAP and attribute values, respectively. Each dot represents one instance and its color informs the density and ratio of classes, as in Fig. 2-b1. From these plots, for example, we can observe that larger open (openness) has a negative impact on the 1D representation reflecting `scoreLevel1`. On the other hand, larger `consci` (conscientiousness) has a positive impact. Moreover, `netaddict` (internet addiction) has clearly different patterns between Class 0 (red, low `scoreLevel1`) and Class 1 (blue, high `scoreLevel1`): larger `netaddict` tends to have a more negative impact for Class 0. As shown in Fig. 4, we also tested different visual designs. Fig. 4-a is based on the default plot in the SHAP Python package [38], where the swarm-plot-like visualization is used, as in Fig. 2-b1. Using  $x$ -coordinates and colors of dots, this visualization informs SHAP and attribute values. From this visualization, we can roughly understand the relationships between the values (e.g., larger open tends to have a more negative SHAP value); however, it is infeasible to know the different patterns between the two classes. Even when jointly using a visualization that color-encodes class labels (see Fig. 4-b), we still cannot clearly see such different patterns. When compared with these, our final design (Fig. 4-c) can clearly depict the

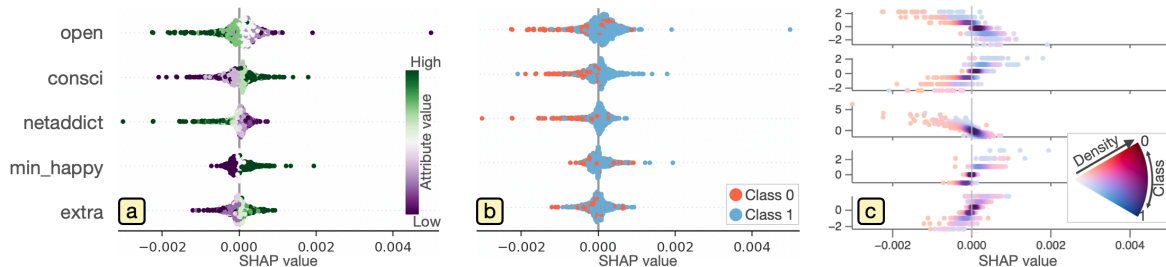


Fig. 4. Design comparison of SHAP value visualizations. Across all visualizations, each row is allocated for one attribute and  $x$ -coordinates represent SHAP values; however, attribute values and/or class labels are encoded differently. (a) The default plot provided in the SHAP Python package [38] encodes attribute values with a divergent colormap while using  $y$ -direction to pile up dots (similar to the swarm-plot-like visualization in Fig. 2-b1). (b) The color of each dot encodes a class label. (c) Our design uses  $y$ -coordinates and colors to represent attribute values and class labels, respectively.

relationships between SHAP and attribute values as well as the different patterns seen in the two classes.

Because each instance has one SHAP value for each attribute, as a global measure of each attribute’s contribution, we use the mean absolute value of all instances’ SHAP values. Then, we sort and display attributes in Fig. 2-a based on their contributions. The analyst can refer to these ordered attributes when selecting attributes for the composite variable construction.

### 3.5.2 Composite Variable Construction

The composite variable is commonly used when using a single attribute is not sufficient to understand a target phenomenon (DC3: Interpretability and DC2: Expressivity). For example, in baseball, on-base plus slugging (OPS)—the sum of two different attributes of the player’s performance, on-base percentage (OBP) and slugging percentage (SLG)—is used to analyze each player’s contributions to team runs or winnings. This is because OPS is a simple composite variable but extremely correlates to team runs [1].

We describe the optimization algorithm designed to construct a composite variable from user-selected attributes. First, we need to define the objective function for the optimization. To explain the 1D representation with the selected attributes as much as possible, we want to obtain the maximum value for a certain “measure of dependence” [52] (i.e., a measure indicating how closely two variables are related). We use either Pearson’s or Spearman’s correlation coefficient as a measure of dependence. Also, we construct a composite variable with a linear combination of attributes for a simple, intuitive interpretation as well as an efficient optimization to allow interactive construction. A linear combination that achieves the highest Pearson’s correlation coefficient can be computed with multivariate linear regression. As Spearman’s involves a non-differentiable operation to rank the 1D representation values, we cannot perform the optimization with simple regression or gradient-based solvers. Thus, we employ a gradient-free solver, specifically COBYLA (or constrained optimization by linear approximations) [50] while using the optimized result for Pearson’s as an initial solution. Although the optimization for Pearson’s is much more efficient, Spearman’s could be more effective in some cases. This is because the 1D representation is constructed from the non-linearly transformed attributes by the NN, and the 1D representation may have a nonlinear correlation with the original input attributes.

With the view in Fig. 2-a, the analyst can select attributes and a measure of dependence, and generate a composite variable by clicking “Construct New Composite Variable” located at the bottom. The selected attributes are highlighted with a gray background. Then, as shown in Fig. 2-b2, the relationships between the 1D representation ( $x$ -axis) and composite variable ( $y$ -axis) are visualized with the two-class density scatterplots described in Sect. 3.5.3. The UI allows the analyst to generate multiple composite variables to compare their expressivity and interpretability (DC4: Tunability). A newly constructed composite variable’s visualization is appended to a list of scatterplots in the scrollable view. The analyst can also discard a scatterplot by clicking a “ $\times$ ” mark at the top right.

In essence, through this composite variable construction process, the analyst can utilize their domain knowledge to review the simplified representation. From the attributes ranked by SHAP values, the analyst can judge attributes they should consider. Then, with the help of the above optimization algorithm, the analyst can interactively examine and fine-tune the composite variables to find useful insights.

For Dataset I analyzed in Fig. 2, Spearman’s correlation coefficient between each of the top-5 contributed attributes and the 1D representation is `open`: -0.147, `consci`: 0.237, `netaddict`: 0.134, `min_happy` (the minimum of 1-hop neighbors’ happiness levels): 0.093, and `extra` (extraversion): 0.026. As shown in Fig. 2-b2, using all the five attributes, we can generate a composite variable that has a better correlation coefficient, 0.300. This is a moderate correlation based on Dancy and Reidy’s categorization [12], which we follow in the rest of the paper when describing correlation strengths. As all attributes are normalized, each attribute’s weight in the composite variable shows the contribution level to the composite variable (`open`: -0.4, `consci`: +0.7, `netaddict`: -0.3, `min_happy`: +0.3, `extra`: +0.3). We can see that `consci` contributes most, as expected from its higher Spearman’s correlation (0.237) than the others. On the other hand, while `extra` has an extremely small correlation (0.026) as a single attribute, a relatively large weight is assigned (+0.3). In fact, when excluding `extra`, the correlation coefficient decreases from 0.300 to 0.289. By checking how the inclusion of `extra` improves on the other attribute’s correlation, we observe that `open` has much larger improvement (from 0.147 to 0.170) than the others (e.g., `consci` has no improvement). From this, we can expect that by including `open` and `extra` with different signs (-0.4 and 0.3), the composite variable captures the subtle difference between these two personalities, which is more related to `scorelevel` than either of `open` or `extra`. We should emphasize that the above insights cannot be derived if only investigating a single attribute relationship to the 1D representation. Also, this example demonstrates the reason for the use of the SHAP method for the attribute recommendation, instead of simply relying on the correlation coefficients.

We should note that while we want to make a composite variable correlated to the 1D representation to some extent (e.g., Spearman’s  $\geq 0.2$ , weakly correlated), we do not have to see highly correlated results (e.g., Spearman’s  $\geq 0.7$ , strongly correlated). If an extremely strong correlation can be found with a linear combination of a few attributes, the use of NNs becomes unnecessary as we can expect linear learning methods such as LDA are sufficient for the prediction. Rather, here we want to take a further step from the single-attribute-based interpretation using the SHAP method or others [33, 39, 44] by providing the interpretation method considering the combinational influence of attributes. Such an influence can be analyzed via the signed weights in a composite variable and the interactive adjustment of the composite variable, as demonstrated above. And, the correlation coefficient can be used as a reference to know how much of the 1D representation is explained with the composite variable.

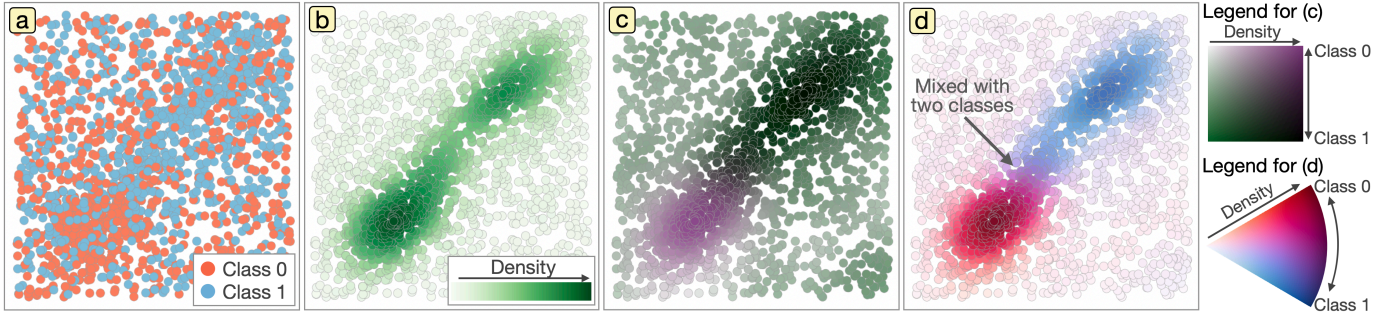


Fig. 5. The comparison of scatterplot designs: (a) scatterplot with colored classes, (b) density scatterplot, (c,d) scatterplots encoding the density and the ratio of each class’s density with two different bivariate colormaps. (d) is our final design for a two-class density scatterplot.

### 3.5.3 Two-class Density Scatterplot

From a scatterplot showing the relationships between the 1D representation and the composite variable, we want to find (1) patterns related to binary classes; (2) trends including correlations; (3) other supplemental patterns, such as noises, outliers, and clusters. For example, we may want to check the quality of the class separation to refine the settings for Steps 1–3, update the attribute selection in Step 5 based on the correlation pattern, or find subgroups for further analyses (e.g., only a subset of instances might have a clear trend).

Based on the survey on scatterplot designs [54], we should employ a visual encoding that involves the aggregation of instances for the identification of trends (especially, correlations) while we should show individual instances for the other tasks (e.g., finding outliers). However, providing an encoding that satisfies these requirements is not straightforward. For example, in Fig. 5-a, the class information is encoded with colors of dots. This encoding easily suffers from overplotting when analyzing a large dataset (e.g., 1000 instances). In Fig. 5-a, it is difficult to find a clear trend hidden by noises. The density scatterplot is effective to find trends, as shown in Fig. 5-b, where the correlated pattern can be seen along the diagonal direction. However, from the density scatterplot, we cannot grasp where each class’s instances are located, and we do not know, for example, whether or not the dense area mostly consists of a single class.

To solve the above issues, as shown Fig. 5-d, we develop a *two-class density scatterplot*, using a bivariate colormap. As shown in its legend, the density and the ratio of each class’s density are encoded with color lightness and hue, respectively. From this plot, we can clearly see the correlated pattern as well as confirm that the two dense areas at the bottom left (more red colors) and top right (more blue colors) mainly consist of a single class. From the purple color area annotated with the arrow in Fig. 5-d, we can also observe that a part of the dense area contains a considerable amount of both classes’ instances. We should note that a bivariate colormap has been already utilized to simultaneously show two different measures over scatterplots (e.g., [36]); however, we introduce the computation of the ratio of each class’s density and select color encoding suitable for showing class and density information with scatterplots.

Similar to an ordinal density scatterplot, we first estimate the 2D probability density function (PDF) from the instances’ coordinates. This can be done by applying a Gaussian kernel density estimation to all instances. Let  $f_{\text{all}}$  denote the 2D PDF estimated with all instances. Then, the density at a 2D coordinate,  $\mathbf{p}$ , can be computed with  $f_{\text{all}}(\mathbf{p})$ . Similarly, let  $f_0$  and  $f_1$  denote 2D PDFs estimated with Class 0’s instances and Class 1’s instances, respectively. Also, let  $n_0$  and  $n_1$  be the numbers of instances in Class 0 and Class 1. Then, a function that estimates the ratio of Class 0’s density at  $\mathbf{p}$  can be written with:  $g_0(\mathbf{p}) = n_0 f_0(\mathbf{p}) / (n_0 f_0(\mathbf{p}) + n_1 f_1(\mathbf{p}))$ . When assigning the same total density for each class is more appropriate for an analysis, instead, we can use  $g_0(\mathbf{p}) = f_0(\mathbf{p}) / (f_0(\mathbf{p}) + f_1(\mathbf{p}))$ .

Now, we encode the density,  $f_{\text{all}}(\mathbf{p})$ , and the ratio of Class 0’s density,  $g_0(\mathbf{p})$ , with a bivariate colormap. We select color lightness to encode the density because of its natural metaphor: The more accu-

mulumation of dots, the denser color. We then employ hue to represent the class ratio. While we tested ordinary HSL and HSV color spaces for this encoding and a similar encoding using saturation instead of lightness, a subtle density difference was difficult to recognize from the generated colors. Thus, we utilize existing carefully designed sequential colormaps, specifically the red and blue sequential colormaps in Matplotlib.<sup>3</sup> We can obtain a pair of colors corresponding to the density from these two colormaps and then generate an interpolated color from the pair based on  $g_0(\mathbf{p})$ . To show this 2D color space as a legend, we use a polar coordinate, as shown at the bottom right of Fig. 5. This is to clearly indicate the difference between the meanings of two measures (density and ratio) as well as to inform that the class ratio difference is less emphasized in low-density areas. As shown in Fig. 5-c, we also tested existing bivariate colormaps such as one introduced in [36]. However, from Fig. 5-c, it is difficult to recognize, for example, Class 1’s high-density area and the density difference between the high-density areas of Class 0 and Class 1.

While we develop the two-class density scatterplot for the views in Fig. 2-b, we employ the same design for Fig. 2-a. As presented in Sect. 3.5.1, the two-class density scatterplot can clearly show patterns of two classes even in the limited plotting space.

## 3.6 Interactive Visual Interface

All the visualizations in the UI are fully linked and share the same or similar color encodings (e.g., red represents Class 0). The user can perform lasso selection in Fig. 2-a, b, c, and the selected instances from Classes 0 and 1 are highlighted in yellow (e.g., Fig. 7-c). With this linking, the analyst can investigate specific patterns, such as outliers and subgroups. In Fig. 2-c and d, we provide visualizations of the dataset’s structural and semantic information to supplement the interpretation of the results.

**Structural information.** We use Fig. 2-c to show network layouts as the structural information of the data.

As the precomputed network measures (e.g., node degree) used for NRL (see Sect. 3.4.1) are computed based on links among all instances, to locate patterns related to the structural information, we need to review the entire network, instead of the subnetwork only consisting of instances in the two ends (i.e., Classes 0 and 1). Thus, only in this view, we visualize all instances including even those not belonging to the two ends. We lay out all instances by scalable force-directed placement (SFDP) [27] and use red, blue, and gray colors to represent Class 0, Class 1, and other instances, respectively. When performing lasso selection in this view, only Class 0 and Class 1 instances inside of the lasso are selected to consistently link with the other views.

**Attribute information.** We visualize the distribution of each attribute as a double-bar histogram. By default, as shown in Fig. 2-d, the UI shows the distribution for each class. When the lasso selection is performed, we show the distributions of selected and non-selected instances (e.g., Fig. 6-b1). As we have limited space, we order histograms based on the two groups’ distribution differences measured by the Kolmogorov–Smirnov (KS) statistic.

<sup>3</sup><https://matplotlib.org/stable/tutorials/colors/colormaps.html>

**Implementation.** The UI is developed as a web application. For the back end, we use Python to perform Step 2 with DeepGL and MLPs, Step 3 with regularized LDA, Step 4 with the SHAP method, Step 5 with multivariate regression and the COBYLA, and Step 6 with the two-class density scatterplot generation, SFDP, and KS statistic. For these algorithms, we utilize various libraries and packages, such as deepgl [19], PyTorch [47] (for MLPs), ulca [17] (for regularized LDA), SHAP [38], Scikit-learn [48] (for multivariate regression), NumPy/SciPy [59] (for the COBYLA, KS statistic, and Gaussian kernel density estimation), graph-tool [49] (for SFDP), seaborn [62] (for the swarm-like visualization), and ColorAide [43] (for color generation). The front-end UI is implemented with a combination of HTML5, JavaScript, and D3 [5]. We use WebSocket to communicate between the front- and back-end modules.

## 4 CASE STUDIES

We demonstrate the effectiveness of our workflow and interactive visualizations with three case studies using the two datasets. For the first two case studies, using Dataset I, we show analyses on network nodes. In the third case, we analyze egocentric networks derived from Dataset II.

### 4.1 Study 1: Associations with Score Levels

Here we describe a complete version of the analysis we have performed in Sect. 3.4 and Sect. 3.5, where we target the identification of attributes that are highly related to college students’ `scorelevel` from Dataset I, which consists of 1886 nodes/students, 64156 links, and 85 node attributes after the preprocessing (see Sect. 3.3 and Sect. 3.4.1). We classify the bottom and top `scorelevel` groups with the five-layer MLP using 128, 64, and 64 NN nodes for the first, second, and third hidden layers, respectively. There are 138 students in the bottom group (Class 0, red color) and 648 students in the top group (Class 1, blue color). The prediction results show 1.0 accuracy for Step 2 but 0.98 for Step 3 (refer to Sect. 3.4.1 for the reason for accepting such a high accuracy in Step 2). Fig. 2 shows the visualized results in the UI.

From the visualization of the 1D representation, as shown in Fig. 2-b1, we first confirm that the learning result via Steps 1–3 provides a reasonable separation between two classes. Also, from the distribution of instances/students, we expect that the 1D representation is not extremely overfitted for this classification (i.e., there is a sufficient variety for the coordinates).

We then review the attributes’ associations with the 1D representation from the view in Fig. 2-a. Based on the ranked order of the attributes, rather than network centralities, we see that attributes more contributing to the score level differences are highly related to many of the Big Five personality traits (i.e., `open` (openness), `consci` (conscientiousness), `extra` (extraversion), `neuro` (neuroticism), and `agree` (agreeableness)) as well as certain statuses, such as `netaddict` (internet addiction level) and `min_happy` (the minimum of the friends’ happiness levels). As we have already examined in Sect. 3.5.1, the top-5 attributes have clear positive or negative trends with the SHAP values (e.g., higher `open` tends to have a more negative SHAP value).

We construct a composite variable with these top-5 attributes to maximize Spearman’s correlation coefficient with the 1D representation, resulting in the visualization shown in Fig. 2-b2. From the equation of the composite variable,  $y = -0.4(\text{open}) + 0.7(\text{consci}) - 0.3(\text{netaddict}) + 0.3(\text{min\_happy}) + 0.3(\text{extra})$ , we see that the attributes’ signs of weights match with their positive or negative influence on the 1D representation, as seen in Fig. 2-a. Based on the magnitudes, we can see `consci` contributes most to the 1D representation. Also, as discussed in Sect. 3.5.2, we observe that `open` and `extra`—personalities that might have some overlapped aspect—likely derive a new meaningful attribute by having opposite signs with each other. More specifically, a composite variable,  $y = -0.9(\text{open}) + 0.4(\text{extra})$ , shows 0.170 correlation coefficient. This indicates that having both openness and introversion tends to have clearer negative impacts on their score levels.

Even though similar information with the attribute combining `open` and `extra` could be captured by the network centralities such as

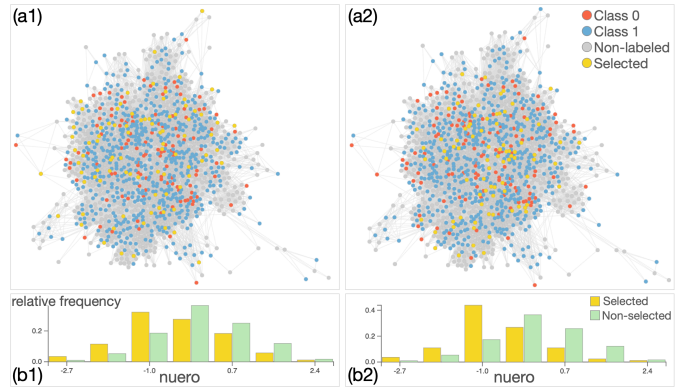


Fig. 6. Study 1: The network layouts after selecting students with (a1) high  $(-0.9(\text{open})+0.4(\text{extra}))$  and (a2) high extra. The distributions of `neuro` (b1, b2) corresponding to the selections of (a1, a2).

node degree (e.g., the students with high `extra` could have more friends), as mentioned, the centralities do not have clear influences on the 1D representation. To examine the relationships between the attribute and network structure, we select students who have low  $(-0.9(\text{open})+0.4(\text{extra}))$  from the UI and update the network layout visualization, as shown in Fig. 6-a1. While we see several selected students (colored yellow) are located on the outskirts (i.e., fewer connections to others), we cannot find any clear structural pattern. When selecting students with high `extra`, as shown in Fig. 6-a2, we cannot see a clear pattern either. Thus, we can say that openness and extraversion in a real life are difficult to capture only from the connections on Facebook. The ordered histograms by their KS scores show that selected and non-selected students have strongly different distributions for `neuro`. From the distributions of `neuro` shown in Fig. 6-b1, b2, the students with high  $(-0.9(\text{open})+0.4(\text{extra}))$  or high `extra` tend to have lower `neuro` than others. Thus, `neuro` also seems to be inter-related to `open` and `extra`; however, based on Fig. 2-a, `neuro` has a smaller influence on the score level and does not show consistent positive or negative influences among students. In fact, we see that the inclusion of `neuro` into the composite variable of the top-5 attributes does not improve its correlation coefficient.

The above observations derive several reasonable insights: The student’s conscientiousness is highly related to their class score; internet addiction has a negative association with the score, especially, for those who had bad scores (refer to Sect. 3.5.1); if all friends have sufficient happiness, the score tends to be higher, and vice versa; and the openness and extraversion show a clear combinational effect and a high openness with a low extraversion has a more negative relationship to the score.

### 4.2 Study 2: Differences by Academic Units

From Dataset I, by changing the classification target of Step 2, we review whether or not students from different majors have different structural and semantic characteristics. To perform this comparison, we select each pair of six different majors recorded in the data (agricultural, business, engineering, humanities, physical sciences, and social sciences). While we have compared all the majors, we show one representative analysis example, where we compare students who major in business (Class 0, red, 801 students) and engineering (Class 1, blue, 287 students). We use the same 85 attributes and MLP as in Study 1. The prediction results show 1.0 accuracy for both Steps 2–3.

Fig. 7-a shows the top-8 attributes contributing to the differences between business and engineering. Unlike Study 1, we can see attributes related to the network structure such as `eigenvector`, `betweenness`, and `total_degree`. To review the relationships between these centralities and the 1D representation, we generate a composite variable with these three centralities. As shown in Fig. 7-b, the resultant composite variable shows a moderate correlation (Spearman’s: 0.511). Also, we can see large weights with opposite signs



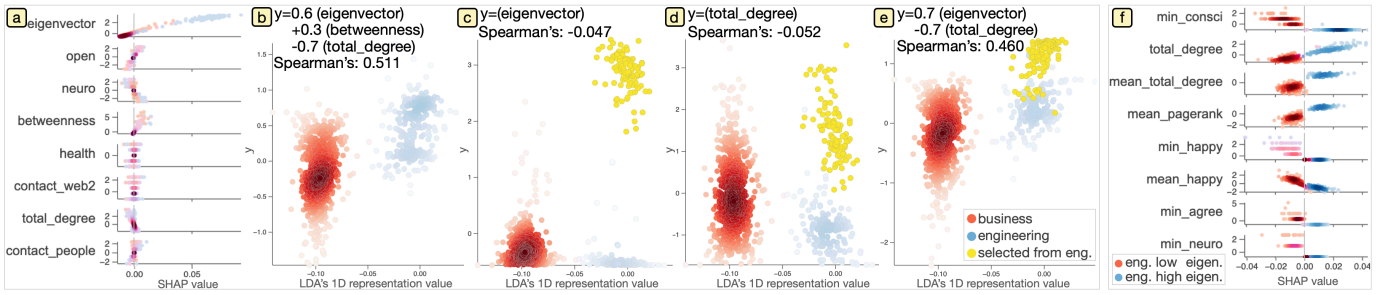


Fig. 7. Study 2: Visualizations for (a-e) the comparison of business and engineering students and (f) the comparison of engineering students with high and low eigenvector centralities.

for eigenvector and total\_degree: +0.6 and -0.7, respectively. As described in Sect. 3.4.1, unlike degree centrality, eigenvector centrality considers the importance of links. Therefore, taking a subtraction of node degree from eigenvector centrality emphasizes the characteristics unique to eigenvector centrality.

As we can see the strong and clear positive influence of high eigenvector from Fig. 7-a, we visualize the relationships between eigenvector and the 1D representation, as shown in Fig. 7-c. We first notice that eigenvector itself has a very small correlation coefficient (-0.047). But, we also identify two clear subgroups in a group of engineering as we highlight one group in yellow. Also, a similar but more moderate separation can be seen in total\_degree (see Fig. 7-d). We then make a new composite variable using only eigenvector and total\_degree. The result shown in Fig. 7-e informs a clear correlation of the composite variable to the 1D representation (0.460). By looking at the visualizations in Fig. 7-c, d, and e, we can observe how this composite variable informative for the difference of business and engineering is generated from the two attributes. Again, finding this type of information is difficult when only reviewing an influence from a single attribute.

We are also interested in the difference between low and high eigenvector groups in engineering students and select these two groups as a classification target. Fig. 7-f shows the top-8 contributing attributes for this classification, where red and blue colors are now used for low and high eigenvector groups. We see that most attributes show a clear separation between the groups and many of them are related to the student’s personality or mentalities, such as consci, happy, and agree. However, we also see that the listed attributes in Fig. 7-f tend to correspond with the minimum values of their friends’, as indicated with the prefix, “min\_”. As the high eigenvector group tends to have high total\_degree as well (see Fig. 7-d), the students in this group have a higher chance to have some friends with low values for any of the survey attributes. Therefore, this result is likely from inappropriate fittings specific to these two groups, and we should further examine their differences, for example, by removing those 1-hop neighbor statistics taking the minimum or maximum.

From this study, we observe the difference between students who major in business and engineering in the composite variable constructed with the network centralities. As the composite variable emphasizes the difference between the eigenvector and total degree centralities, we can say that engineering students tend to have connections more specific to influential students in Facebook. Also, we demonstrate the case of identifying potential inappropriate overfitting from the visualized results.

### 4.3 Study 3: Factors Promoting New Connections

Using Dataset II, we generated multivariate egocentric networks by adding 1- and 2-hop neighbors of the survey respondent based on the contact records (i.e., 1-hop: direct contacts, 2-hop: indirect contacts) as well as network-level attributes, such as the ego node’s personality, Facebook usage statistics, and network measures (e.g., clustering coefficient). Also, we have an attribute informing whether or not an indirect contact became a direct contact from January 1, 2015 to June

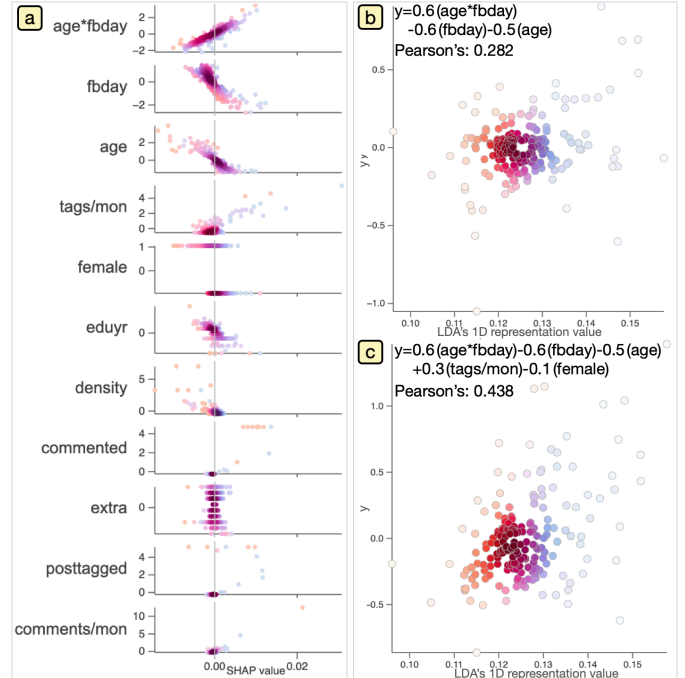


Fig. 8. Study 3: (a) The top contributing attributes and composite variables constructed with (b) the top-3 and (c) top-5 attributes.

30, 2017. The resultant egocentric networks consist of 345 ego nodes, 3339 1-hop neighbors, and 19917 2-hop neighbors.

To identify contributing attributes to the transformation from indirect contacts to direct contacts, we first compute the transformation rate  $r$  for each network (i.e., the ratio of the number of indirect contacts transformed to direct contacts during the study period). We then respectively select respondents with conditions of  $r=0$  (i.e., no transformation) and  $r \geq 0.2$  (i.e., high transformation rate) as Class 0 (red, 56 respondents) and Class 1 (blue, 136 respondents). The accuracies for Steps 2 and 3 are 1.0 and 0.82, respectively.

Fig. 8-a shows the top-10 attributes contributing to the 1D representation. Similar to the other studies, we see several clear trends between each attribute’s values and the SHAP values. For example, age\*fbday (multiplication of the ego’s age and total days of Facebook use, fbday)—the predefined composite variable in the existing study [35]—shows an increasing trend (i.e., larger age\*fbday has a more positive impact on the transformation). As all the top-3 attributes, age\*fbday, fbday, age, are likely inter-related, we construct a composite variable with these attributes. The result is shown in Fig. 8-b, where the composite variable,  $y=0.6(\text{age} * \text{fbday}) - 0.6(\text{fbday}) - 0.5(\text{age})$ , has a weak correlation (Pearson’s: 0.282). When we investigate three attributes individually, we notice that they have much lower correlation coefficients to the 1D representation than this composite variable

(age\*fbday: 0.064, fbday: 0.052, age: 0.123). Thus, the composite variable seems to find meaningful information by disentangling the complicated relationships among the three attributes. We further construct a composite variable by adding tags/mon (the average times of being tagged per month) and female (whether ego’s gender is female or not). As shown in Fig. 8-c, the resultant composite variable using these attributes significantly improves the correlation coefficient from the previous one (from 0.282 to 0.438).

As a verification, we compare our findings with the existing study [35], where the researchers employed a mixed-effect model to measure each attribute’s influence on the transformation of indirect contacts. The top-5 influential attributes suggested by their model are female, extra, comments/mon (the average number of comments made per month), fbday, and age\*fbday. First of all, three attributes are seen in both their results and ours (i.e., age\*fbday, fbday, and female). Also, we can expect that tags/mon and comments/mon have similar influences based on their meanings. In fact, when replacing tags/mon with comments/mon for the composite variable construction, we obtain the composite variable with 0.382 Pearson’s correlation coefficient, which is considerably close to the original (Pearson’s 0.438). From these observations, we can expect that our NN-based model has successfully captured similar information to the statistical model used in [35]. Moreover, the unique strength of our approach is that we can see the inter-relationships of attributes from their weights in the composite variable. As discussed, we can suggest  $0.6(\text{age}^*\text{fbday}) - 0.6(\text{fbday}) - 0.5(\text{age})$  or a more simplified version,  $\text{age}^*\text{fbday} - \text{fbday} - \text{age}$ , as a potential composite variable to better capture the influence on the transformation than  $\text{age}^*\text{fbday}$ , which is used in the aforementioned work.

## 5 EXPERT FEEDBACK

To further validate our workflow’s usability, we conducted an informal interview with experts in social network studies. The first expert (E1) is a distinguished researcher in an institute of sociology who collected the datasets used in our case studies and also conducted research on the same datasets with different focuses. The second expert (E2) is an assistant professor in a department of sociology who formulated the guidelines for collecting the datasets. The other three experts are researchers in institutes of sociology (E3) and statistical science (E4, E5) who also studied the same datasets. The interview was conducted through a video conference setup, where the preliminary versions of the three case studies were presented.

All the experts agreed that our workflow can support a wide range of their analysis targets as well as derive more insights with intuitive interpretations when compared to their current approaches employing statistical models. For example, E1 commented, “The results [seen in the composite variables] are much easier to understand and intuitive than the outputs from the statistical models used in our previous research.” All of them showed strong interest in insights that can be derived from the signed weights in composite variables. We presented some of such insights in the case studies. On the other hand, E1 noted a potential limitation of the dataset and analyses: “The distribution of the respondents might affect the results related to the internet addiction (netaddict), as the students who granted the use of their data tended to be more addicted to the internet usage than others.” E2 suggested better selections of input attributes for the analyses, and we improved our case studies, accordingly.

There are several discussions on our workflow usage and design. E3 asked, “What if there are attributes with a dominant influence on the result? What if the 1D representation does not have clear separation?” For the former, to identify such attributes, analysts can refer to the visualization of shown in Fig. 2-a and update the inputs if dominant attributes exist. Similarly, for the latter case, the visualization shown in Fig. 2-b1 is useful to review the degree of the separation, and based on the result, analysts can take actions, such as adding more input attributes, reducing the ranges of the two ends of the output attribute, and improving the NN model. E4 raised a question on our post-hoc simplification of network representations: “Why not only use a neural network by designing the last layer with a linear activation function,

instead of using LDA?” Our answer is stated in Sect. 3.4.2. E5 asked, “Why not use other centralities but these three?” We selected degree, eigenvector, and betweenness centralities as a set of the most fundamental measures of structural characteristics. However, our workflow is flexible to employ any other set of centralities based on analysts’ research interests.

## 6 DISCUSSION

Through the case studies and the expert interview, we have shown the effectiveness of our workflow and interactive visualizations. Here, we provide additional discussions on our designs.

**Applicability to various data types.** We have designed our workflow for multivariate networks. As multivariate networks have both high-dimensional and relational characteristics, by its nature, the workflow can be applicable to high-dimensional data and univariate network data. For example, we can analyze high-dimensional data by skipping the computation of the network centralities and  $k$ -hop neighbor statistics and the visualization of networks. In addition, our workflow design can potentially adapt to advanced models of networks such as those containing meta-nodes and hyperedges. For example, as long as meta-nodes have the same set of node attributes as simple nodes in a network, we can still apply the same processes in our workflow. Also, our workflow precomputes node and link-related features before the training utilizing NNs; thus, we can deal with hyperedges during this preprocessing step (e.g., in DeepGL, by including hyperedges as links that should be considered for the selection of neighbor nodes).

**Other potential algorithm designs.** While we employ the NNs, DR, and composite variable construction to support the aforementioned analysis target, there are other potential designs. One common way to understand the associations among a target and other attributes is using a decision tree (DT) [6, 37]. When compared with a DT-based analysis, our design provides two main strengths in the interpretation step: simplicity and informativity. A DT provides a set of conditions of attributes’ ranges that can classify a target attribute. However, the number of conditions would be easily overwhelming when analyzing networks with many attributes. Also, from the DT’s result, it is difficult to numerically identify the combinational influence from multiple attributes, such as those seen in the composite variables we have constructed for the case studies.

Another possible design is allowing for the construction of more complicated composite variables, for example, by allowing to take multiplications and/or logarithms of attributes. Although this would be more effective when analyzing complex relationships among attributes (e.g., age and fbday in Sect. 4.3), this construction requires much more complicated optimizations than ours. One potential way to perform such advanced constructions while avoiding excessive computation is incorporating analysts’ knowledge by enabling them to interactively build a part of the composite variable (e.g., inputting an equation template for the composite variable). We plan to investigate this direction in future research.

**Usability of two-class density scatterplots.** We have developed the two-class density scatterplot to examine various important patterns (e.g., distributions of class instances, trends, clusters, and outliers) with a single visualization. The usage of this scatterplot is not limited to the targeted analyses in this work. As binary classifications or group comparisons are frequently performed for machine learning and visual analytics, we believe the two-class density scatterplot can widely contribute to these fields. As future research, we would like to conduct a comprehensive user study to evaluate the effectiveness of our scatterplot design as well as to identify its shortcomings for further improvements.

As its name indicates, the two-class density scatterplot is designed only for visualizing two classes. One potential design for three or more classes is taking similar approaches to the multiclass (geographical) maps by Jo et al. [28]. For example, we can first partition a 2D space by the change in the class distribution and then display a distribution of classes in each partitioned region with a bar-chart glyph. We expect that this design can deal with several classes (e.g., five classes); however, this partition-based approach would not be suitable to reveal outliers and clusters. Thus, we also would like to investigate a better design for

three or more classes in the future.

## 7 CONCLUSION

We have introduced a new visual analytics workflow designed to help find associations from complex multivariate networks. The workflow integrates neural-network-based representation learning, composite variable construction, and interactive visualizations. Benefiting from these components, the workflow generates expressive as well as interpretable analytical results. The design of workflow is also suited for analyzing other simpler types of data, such as a univariate network and high-dimensional data. Thus, our work potentially contributes to a wide range of applications that involve analyses of large, complex data.

## ACKNOWLEDGMENTS

This work has been supported in part by the National Institute of Health through grants 1R01CA270454-01 and 1R01CA273058-01 and by the Knut and Alice Wallenberg Foundation through Grant KAW 2019.0024.

## REFERENCES

- [1] J. Albert. Sabermetrics: The past, the present, and the future. In J. A. Gallian, ed., *Mathematics and Sports*, p. 3–14. Mathematical Association of America, 2010.
- [2] M. Atzmueller, S. Günnemann, and A. Zimmermann. Mining communities and their descriptions on attributed graphs: A survey. *Data Min Knowl Disc*, 35(3):661–687, 2021.
- [3] B. Bach, C. Shi, N. Heulot, T. Madhyastha, T. Grabowski, and P. Dragicevic. Time Curves: Folding time to visualize patterns of temporal evolution in data. *IEEE Trans Vis Comput Graph*, 22(1):559–568, 2016.
- [4] F. Beck, M. Burch, S. Diehl, and D. Weiskopf. A taxonomy and survey of dynamic graph visualization. *Comput Graph Forum*, 36(1):133–159, 2017.
- [5] M. Bostock, V. Ogievetsky, and J. Heer. D<sup>3</sup> data-driven documents. *IEEE Trans Vis Comput Graph*, 17(12):2301–2309, 2011.
- [6] J. E. Brand, J. Xu, B. Koch, and P. Geraldo. Uncovering sociological effect heterogeneity using tree-based machine learning. *Sociol Methodol*, 51(2):189–223, 2021.
- [7] M. Cavallo and Ç. Demiralp. A visual interaction framework for dimensionality reduction based data exploration. In *Proc. CHI*, pp. 1–13, 2018.
- [8] M.-y. Chang and Y.-c. Fu. Social media and network boundaries among college students: Reconstructing companions, conversations, and contact circles. *Taiwanese Sociology*, 37:1–46, 2019. (in Chinese).
- [9] A. Chatzimpampas, R. M. Martins, I. Jusufi, K. Kucher, F. Rossi, and A. Kerren. The state of the art in enhancing trust in machine learning models with the use of visualizations. *Comput Graph Forum*, 39(3):713–756, 2020.
- [10] A. Chatzimpampas, R. M. Martins, and A. Kerren. t-viSNE: Interactive assessment and interpretation of t-SNE projections. *IEEE Trans Vis Comput Graph*, 26(8):2696–2714, 2020.
- [11] R. Chetty, M. O. Jackson, T. Kuchler, J. Stroebel, N. Hendren, et al. Social capital I: Measurement and associations with economic mobility. *Nature*, 608:108–121, 2022.
- [12] C. P. Dancy and J. Reidy. *Statistics without maths for psychology*. Pearson London, 2017.
- [13] R. Faust, D. Glickenstein, and C. Scheidegger. DimReader: Axis lines that explain non-linear projections. *IEEE Trans Vis Comput Graph*, 25(1):481–490, 2018.
- [14] M. Freire, C. Plaisant, B. Shneiderman, and J. Golbeck. ManyNets: An interface for multiple network analysis and visualization. In *Proc. CHI*, pp. 213–222, 2010.
- [15] T. Fujiwara, J.-K. Chou, A. M. McCullough, C. Ranganath, and K.-L. Ma. A visual analytics system for brain functional connectivity comparison across individuals, groups, and time points. In *Proc. PacificVis*, pp. 250–259, 2017.
- [16] T. Fujiwara, O.-H. Kwon, and K.-L. Ma. Supporting analysis of dimensionality reduction results with contrastive learning. *IEEE Trans Vis Comput Graph*, 26(1):45–55, 2020.
- [17] T. Fujiwara, X. Wei, J. Zhao, and K.-L. Ma. Interactive dimensionality reduction for comparative analysis. *IEEE Trans Vis Comput Graph*, 28(1):758–768, 2022.
- [18] T. Fujiwara, J. Zhao, F. Chen, and K.-L. Ma. A visual analytics framework for contrastive network analysis. In *Proc. VAST*, pp. 48–59, 2020.
- [19] T. Fujiwara, J. Zhao, F. Chen, Y. Yu, and K.-L. Ma. Network comparison with interpretable contrastive network representation learning. *J Data Science, Statistics, and Visualisation*, 2(5), 2022.
- [20] M. Gleicher. Explainers: Expert explorations with crafted projections. *IEEE Trans Vis Comput Graph*, 19(12):2042–2051, 2013.
- [21] R. Gove. Gragnostics: Fast, interpretable features for comparing graphs. In *Proc. IV*, pp. 201–209, 2019.
- [22] A. Grover and J. Leskovec. node2vec: Scalable feature learning for networks. In *Proc. KDD*, pp. 855–864, 2016.
- [23] Y. Guo, T. Hastie, and R. Tibshirani. Regularized linear discriminant analysis and its application in microarrays. *Biostat*, 8(1):86–100, 2007.
- [24] W. Hamilton, Z. Ying, and J. Leskovec. Inductive representation learning on large graphs. In *Proc. NIPS*, pp. 1024–1034, 2017.
- [25] R. Hamon, H. Junklewitz, and I. Sanchez. Robustness and explainability of artificial intelligence. Technical Report KJ-NA-30040-EN-N (online), Publications Office of the European Union, 2020.
- [26] M. Harrigan, D. Archambault, P. Cunningham, and N. Hurley. EgoNav: Exploring networks through egocentric spatializations. In *Proc. AVI*, pp. 563–570, 2012.
- [27] Y. Hu. Efficient, high-quality force-directed graph drawing. *Math J*, 10(1):37–71, 2005.
- [28] J. Jo, F. Vernier, P. Dragicevic, and J.-D. Fekete. A declarative rendering model for multiclass density maps. *IEEE Trans Vis Comput Graph*, 25(1):470–480, 2018.
- [29] P. Joia, F. Petronetto, and L. G. Nonato. Uncovering representative groups in multidimensional projections. *Comput Graph Forum*, 34(3):281–290, 2015.
- [30] A. Kerren, H. C. Purchase, and M. O. Ward, eds. *Multivariate Network Visualization*, vol. 8380 of *Lect Notes Comput Sci*. Springer, 2014.
- [31] T. N. Kipf and M. Welling. Semi-supervised classification with graph convolutional networks. *arXiv:1609.02907*, 2016.
- [32] J. Knittel, A. Lalama, S. Koch, and T. Ertl. Visual neural decomposition to explain multivariate data sets. *IEEE Trans Vis Comput Graph*, 27(2):1374–1384, 2020.
- [33] B. C. Kwon, B. Eysenbach, J. Verma, K. Ng, C. De Filippi, W. F. Stewart, and A. Perer. Clustervision: Visual supervision of unsupervised clustering. *IEEE Trans Vis Comput Graph*, 24(1):142–151, 2018.
- [34] O.-H. Kwon, T. Crnovrsanin, and K.-L. Ma. What would a graph look like in this layout? a machine learning approach to large graph visualization. *IEEE Trans Vis Comput Graph*, 24(1):478–488, 2018.
- [35] H.-W. Lee, M.-Y. Chang, W.-Y. Chou, J.-S. Hwang, and Y.-C. Fu. From indirect to direct contacts on Facebook: A big-data approach to the making of triadic network closure. *Can Rev Sociol*, 59(2):207–227, 2022.
- [36] S. Lespinats and M. Aupetit. CheckViz: Sanity check and topological clues for linear and non-linear mappings. *Comput Graph Forum*, 30(1):113–125, 2011.
- [37] Y. Li, E. Musabandesu, T. Fujiwara, F. J. Loge, and K.-L. Ma. A visual analytics system for water distribution system optimization. In *Proc. VIS*, pp. 126–130, 2021.
- [38] S. Lundberg. SHAP (SHapley Additive exPlanations). <https://github.com/slundberg/shap>, 2018. Accessed: 2022-12-28.
- [39] S. M. Lundberg and S.-I. Lee. A unified approach to interpreting model predictions. In *Proc. NIPS*, vol. 30, 2017.
- [40] R. M. Martins, G. F. Andery, H. Heberle, F. V. Paulovich, A. de Andrade Lopes, H. Pedrini, and R. Minghim. Multidimensional projections for visual analysis of social networks. *J Comput Sci Technol*, 27(4):791–810, 2012.
- [41] R. M. Martins, J. F. Krueger, R. Minghim, A. C. Telea, and A. Kerren. MVN-Reduce: Dimensionality reduction for the visual analysis of multivariate networks. In *Proc. EuroVis*, pp. 13–17, 2017.
- [42] F. Mcgee, M. Ghoniem, G. Melançon, B. Otjacques, and B. Pinaud. The state of the art in multilayer network visualization. *Comput Graph Forum*, 38(6):125–149, 2019.
- [43] I. Muse. ColorAide. <https://facelessuser.github.io/coloraide/>, 2020. Accessed: 2022-12-29.
- [44] M. P. Neto and F. V. Paulovich. Multivariate data explanation by jumping emerging patterns visualization. *arXiv:2106.11112*, 2021.
- [45] M. Newman. *Networks*. Oxford University Press, 2018.
- [46] C. Nobre, M. Meyer, M. Streit, and A. Lex. The state of the art in visualizing multivariate networks. *Comput Graph Forum*, 38(3):807–832, 2019.
- [47] A. Paszke, S. Gross, F. Massa, A. Lerer, J. Bradbury, et al. PyTorch:

- An imperative style, high-performance deep learning library. In *Proc. NeurIPS*, pp. 8024–8035, 2019.
- [48] F. Pedregosa, G. Varoquaux, A. Gramfort, V. Michel, B. Thirion, et al. Scikit-learn: Machine learning in Python. *J Mach Learn Res*, 12:2825–2830, 2011.
- [49] T. P. Peixoto. The graph-tool python library. *figshare*, 2014. [http://figshare.com/articles/graph\\_tool/1164194](http://figshare.com/articles/graph_tool/1164194).
- [50] M. J. Powell. Direct search algorithms for optimization calculations. *Acta Numerica*, 7:287–336, 1998.
- [51] N. Pržulj. Biological network comparison using graphlet degree distribution. *Bioinformatics*, 23(2):e177–e183, 2007.
- [52] Y. A. Reshef, D. N. Reshef, H. K. Finucane, P. C. Sabeti, and M. Mitzenmacher. Measuring dependence powerfully and equitably. *J Mach Learn Res*, 17(1):7406–7468, 2016.
- [53] R. A. Rossi, R. Zhou, and N. Ahmed. Deep inductive graph representation learning. *IEEE Trans Knowl Data Eng*, 32(3):438–452, 2018.
- [54] A. Sarikaya and M. Gleicher. Scatterplots: Tasks, data, and designs. *IEEE Trans Vis Comput Graph*, 24(1):402–412, 2018.
- [55] H. Song, Z. Dai, P. Xu, and L. Ren. Interactive visual pattern search on graph data via graph representation learning. *IEEE Trans Vis Comput Graph*, 28(1):335–345, 2022.
- [56] M.-K. Song, F.-C. Lin, S. E. Ward, and J. P. Fine. Composite variables: When and how. *Nurs Res*, 62(1):45, 2013.
- [57] C. Turkay, A. Lundervold, A. Lundervold, and H. Hauser. Representative factor generation for the interactive visual analysis of high-dimensional data. *IEEE Trans Vis Comput Graph*, 18(12):2621–2630, 2012.
- [58] S. van den Elzen, D. Holten, J. Blaas, and J. J. van Wijk. Reducing snapshots to points: A visual analytics approach to dynamic network exploration. *IEEE Trans Vis Comput Graph*, 22(1):1–10, 2016.
- [59] P. Virtanen, R. Gommers, T. E. Oliphant, M. Haberland, et al. SciPy 1.0: Fundamental algorithms for scientific computing in Python. *Nat Methods*, 17:261–272, 2020.
- [60] T. von Landesberger, M. Gerner, and T. Schreck. Visual analysis of graphs with multiple connected components. In *Proc. VAST*, pp. 155–162, 2009.
- [61] M. Waskom. `seaborn.swarmplot`. <https://seaborn.pydata.org/generated/seaborn.swarmplot.html>, 2016. Accessed: 2022-12-27.
- [62] M. L. Waskom. `seaborn`: statistical data visualization. *J Open Source Softw*, 6(60):3021, 2021.
- [63] C. Ying, T. Cai, S. Luo, S. Zheng, G. Ke, D. He, Y. Shen, and T.-Y. Liu. Do transformers really perform badly for graph representation? In *Proc. NeurIPS*, vol. 34, pp. 28877–28888, 2021.
- [64] D. Zhang, J. Yin, X. Zhu, and C. Zhang. Network representation learning: A survey. *IEEE Trans Big Data*, 6(1):3–28, 2018.
- [65] F. Zhou, J. Li, W. Huang, Y. Zhao, X. Yuan, X. Liang, and Y. Shi. Dimension reconstruction for visual exploration of subspace clusters in high-dimensional data. In *Proc. PacificVis*, pp. 128–135, 2016.
- [66] J. Y. Zou, D. J. Hsu, D. C. Parkes, and R. P. Adams. Contrastive learning using spectral methods. *Proc. NIPS*, 26, 2013.